Identification of horizontal slug flow structures for application in selective cross-correlation metering

Drury, R., Hunt, A. & Brusey, J.

Original citation & hyperlink:
Drury, R, Hunt, A & Brusey, J 2019, 'Identification of horizontal slug flow structures for application in selective cross-correlation metering' Flow Measurement and Instrumentation, vol. 66, pp. 141-149.
https://dx.doi.org/10.1016/j.flowmeasinst.2018.12.002

DOI 10.1016/j.flowmeasinst.2018.12.002
ISSN 0955-5986
ESSN 1873-6998

Publisher: Elsevier

Identification of horizontal slug flow structures for application in selective cross-correlation metering

Ross Drury, Andrew Hunt, James Brusey

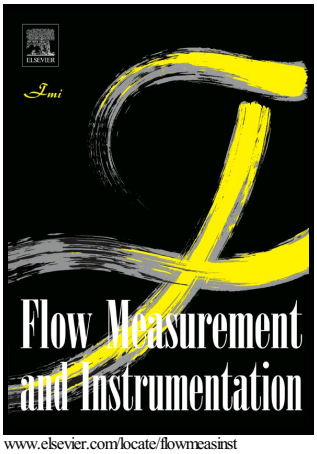

www.elsevier.com/locate/flowmeasinst

PII: S0955-5986(18)30054-2
DOI: https://doi.org/10.1016/j.flowmeasinst.2018.12.002
Reference: JFMI1513

To appear in: *Flow Measurement and Instrumentation*

Received date: 21 February 2018
Revised date: 27 June 2018
Accepted date: 3 December 2018

Cite this article as: Ross Drury, Andrew Hunt and James Brusey, Identification of horizontal slug flow structures for application in selective cross-correlation metering, *Flow Measurement and Instrumentation,* https://doi.org/10.1016/j.flowmeasinst.2018.12.002

Identification of horizontal slug flow structures for application in selective cross-correlation metering

Ross Drury, Andrew Hunt, James Brusey

Abstract

Accurate metering of slug flows is important in many industries that handle multiphase products. For the oil and gas industry the harsh environmental conditions mean that non-invasive and non-intrusive instruments are preferred. Cross-correlation meters, particularly those based on electrical tomography, offer a potential solution to this problem but sufficient accuracy has proved difficult to achieve, with the primary issue being that the measurement is dominated by the motion of interfaces rather than the bulk fluid. In the work reported here, results are presented for flows of oil and nitrogen gas in a horizontal pipe of diameter 10.2 cm. Superficial velocities of liquid and gas range from 1 m/s to 3 m/s and 0.4 m/s to 3 m/s respectively. By analysing the structures of liquid slugs via tomography, it is found that three significantly different slug front structures occur. The high-speed and spatial resolution of Electrical Capacitance Tomography (ECT) enables independent measurement of individual slug fronts and tail as well as average slug velocity. Based on detailed measurements of slug structures and velocity profiles, we go on to show that using differential-based cross-correlation and the average velocity of slug front and tail, an overall accuracy of better than $+/-5\%$ is achieved for estimation of the mixture superficial velocity. This is an equivalent level of accuracy to that obtained using intrusive methods such as optical fibre probes, which are less suitable for oil and gas applications.

Keywords: electrical capacitance tomography, slug flow, two-phase, cross-correlation, translational velocity, slug front, slug tail.

1. Introduction

Multi-phase flows exist within a large range of industries, including chemical, process, nuclear, and oil and gas. The accurate and reliable metering of such flows are therefore important in all these cases, and give the potential for large financial benefits where they can be applied. A potent example can be seen within the oil and gas industry, where, traditionally, multiphase mixtures obtained at oil wells require separation to occur at the well, to allow single phase measurement of the components. Despite the benefit of increased accuracy of single phase measurement, the separation process is itself costly, due to required equipment, and inefficient, compared with merging the process at fewer locations.

Slug flow is a common phenomena in industrial multiphase flows, caused by the effect of the Kelvin-Helmholtz instability on waves at the fluid/gas interface [1]. The effects of oscillating temperature and pressure caused by this flow pattern has promoted much research into the modeling, and in some applications, the prevention of slugging. Despite this, it is accepted that such procedures can be unreliable and lead to loss in production [2], and hence the need for accurate measurement of slug flows will continue.

For measurement and analysis of two phase slug flow, many experimental techniques are available, including high speed cameras (with transparent pipe sections) [3], acoustic emission [4], optical fibre probes [5], wire mesh sensor [6], capacitive sensors [7, 8] and ultrasonic doppler sensors [9] to name a few. Despite these techniques being viable in their own right, when considering applications in environments encountered in the oil and gas industry, there remain some issues. For example, transparent pipes required for visual techniques are not feasible for most applications. Similarly, probes and sensors requiring direct contact with the fluid cause maintenance issues due to the harsh environment encountered, and many newly developed devices currently lack the capability to measure fast enough for industrial flows. Ultrasonics based methods overcome, in part, these issues. The probes are usually integrated into the pipe wall, and despite not interrupting the flow, they can be prone to deposit build-up and have costly maintenance issues. Clamp-on ultrasonic techniques can be problematic for certain flow regimes such as stratified, due to sensitivity to flow profiles [10].

Electrical Capacitance Tomography (ECT) is an example of a device suitable for such applications [11], due to its non-intrusive and non-invasive nature, mature development stage, and relatively low cost. There is also a distinct advantage in using ECT in comparison to simply a capacitive sensor, as it facilitates the ability to conduct more advanced cross correlation techniques, as discussed later in this paper. Furthermore, tomographic devices possess the additional ability of flow regime detection [12, 13], which could be used in conjunction, to develop a gen-

eralised approach to multiphase metering in the future. Cross-correlation flowmeters have been demonstrated as a powerful tool in multiphase flow measurement [14, 15], where fluctuating signals are measured at two separate locations via probe sensors, or non-intrusive techniques such as ECT. The time delay between correlated signals can be used along with the distance between sensors to obtain a velocity measurement. This is viable if the distance between sensors is short enough to ensure minimal change in the flow structure [16], while conforming to the restriction posed by the sampling frequency, and image reconstruction time of the instrument [17].

In the application of cross-correlation to measure slug velocity, the window of integration can be extended or shortened, depending on the amount of data being included in the process. Larger correlation windows have been used to obtain average correlation of multiple liquid slug signals [18], which is attractive in unstable cases, for example, when closer to transition zones between different flow regimes, where slugs are non-uniform in length and frequency. Alternatively, a smaller window, though still longer than the slug duration, can provide individual slug velocity measurement [5] whilst maintaining a strong 'pulse like' signal, which is more suitable for cross-correlation. Although the different integration windows described may be most suited to continuous slug velocity measurement, the most informative technique is to consider separately the slug fronts and tails [19, 20]. The measured slug front and tail velocities are then either treated separately, or an averaged value is used as the measured translational velocity [21]. Finally, care must be taken to ensure that the signal produced by either front or tail, is representative of the actual slug velocity [20].

The application of the discussed methods to recover the mixture velocity has been achieved using a range of instrumentation, although the specific correlation techniques tend to be similar. Zhang and Dong [22] used a resistance based tomography device and cross correlated the raw voltage data, as opposed to a reconstructed image, obtaining an error margin of 10% with a noticeably better accuracy for mixture velocities less than $2m/s$. However, their method included using sample data to construct a coefficient matrix to assist the measurement. Reis and Goldstein [23] achieved a greater accuracy for a larger range of mixture velocities for steady points using a capacitance method, though tests conducted near the flow regime transition zone gave large discrepancies, which were attributed to velocity discontinuities along the gas / liquid flow. Ahmed [24], also used a capacitance sensor for investigation of slug flows, obtaining a more reliable linear trend between slug translational velocity and mixture velocity but with a noticeable deviation for higher mixture velocities, as with Zhang and Dong [22], as well as for low tested values of mixture velocity ($< 0.5m/s$). Van Hout *et al.* [5] went further to analyse the effect of pipe inclination angle on such measurements, and successfully derived a model to account for dispersed bubble within the liquid slug region, achieving an overall a prediction within 15% of the measured flowrates. The deviation in these results was relatively low, which can be attributed to the use of fibre optic probes being intrusive to the flow, and hence not a suitable solution for the environments encountered in many applications.

The main aim of this paper is to evaluate the different methods of applying cross-correlation to slug flows in order to achieve the best possible measurement accuracy. This entails an assessment of how the structure of the slug front and tail affects the measurement and thus, which structures give representative measurements, and the best technique for each distinguishable type of slug structure.The results for estimating the mixture velocity for both the conventional and selective techniques can then be compared to other work.

2. Experimental set-up

Flow loop

Tests conducted in this work were performed on the multi-phase flow loop at the National Engineering Laboratory (NEL) Glasgow, UK. The flow loop is depicted in Figure 1, consisting of a test section of internal pipe diameter 0.102m, and a large gravity separator system. It is capable of delivering refined oil at rates up to $140m^3/hr$ with an uncertainty of $< 1\%$, and gas at rates of up to $600m^3/hr$ with an uncertainty of $< 1.5\%$. The line pressure in the flow loop can operate within a gauge pressure of 0 to $15bar(g)$, and the line temperature can be maintained within the range of 5 to $55°C$, with the controlled temperature and the fluid properties monitored at each test point

The fluids are transported via centrifugal pumps, and reference flow measurements of each phase are taken prior to mixing by turbine meters, calibrated and traceable to the UK national standard. The test section is a horizontal transparent acrylic pipe with a 20mm wall thickness, mounted with the clamp-on ECT device. The range of

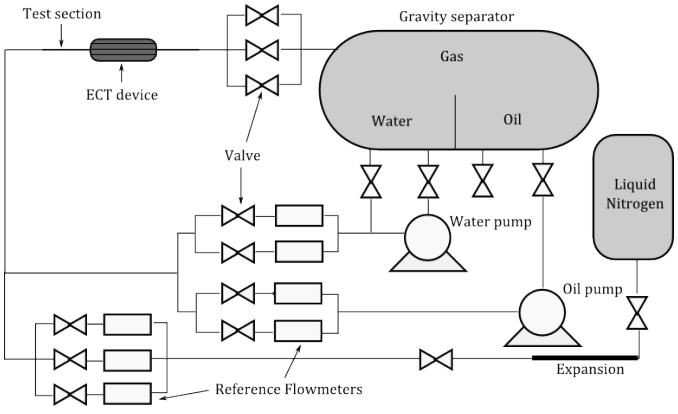

1.png

Figure 1: Schematic of Multi-phase flow rig at the National Engineering Laboratory (NEL), Glasgow, UK.

component velocities used for this work span between 1 m/s to 3 m/s for liquid superficial velocity, and 0.4 m/s to 3 m/s for gas superficial velocity. The oil used in the experiments is ParaFlex HT9 with a stated density $\rho_l = 830kg/m^3$ and viscosity $\mu_l = 18cP$, along with nitrogen gas. During the experiments, temperature in the flow loop varied between 20.7 and 23.5°C, causing a density range of 829.1 to 831kg/m^3, along with a viscosity range of 15.88 to 17.87cP, therefore a minimal effect of temperature variation on the fluid properties and flow regimes is provided within the flow loop.

ECT system

The system used for measurements in this work is a clamp-on, 8 electrode, dual plane ECT system provided by *Atout Process Ltd.*, consisting of the sensor, capacitance measurement system and a control PC, along with dedicated software for analysis. The capacitance measurement system has the capability of sampling at 5 kHz [25], although this was reduced in the current work to reduce data size, while maintaining sufficient temporal resolution of the capacitance measurements. The sensor operates by multiplexing measurements between each electrode pair (giving 28 independent measurements) to give a capacitance reading. The values are then converted into images through the use of pre-calculated sensitivity maps and LBP (Linear Back Projection) as an image reconstruction technique. A technical summary of the ECT sensor is provided in Table 1, and details of the capacitance measurement system are shown in Table 2. The distance between the two measurement planes in the ECT sensor is 6.8cm, this is small enough to ensure that the fluid structures remain similar at both measurement points, without adversely affecting the principle design of the sensor [16]. The images can then provide information about both phase fractions and distribution, (allowing analysis of flow regimes and slug structures) as well as the ability to cross-correlate the images, or specific zones within the image as required. The device is portrayed in use on the multiphase flowloop at NEL in Figure 2.

Property	Value
Type	APL-S-SL-140
Nominal sensor I.D	0.14m
Number of measurement planes	2
Number of electrode segments	8
Total electrically guarded length	0.225m
Axial length of measurement electrode	0.032m
Axial seperation of measurement planes	0.068m

Table 1: Technical summary of the ECT sensor.

Property	Value
Type	TFLR5000
Capacitance measurement range	6fF - 400fF
Maximum image capture rate	1500 fps
Measurement resolution	$<$ 0.1fF
Measurement noise level	$<$ 0.03fF RMS
Communication	Ethernet
Excitation frequency (square wave)	2.5MHz

Table 2: Technical summary of capacitance measurement system (data acquisition hardware).

2.png

Figure 2: Electrical Capacitance Tomography (ECT) sensor provided by *Atout Process Ltd.* in operation at NEL.

Prior to testing, the ECT system requires a calibration procedure. This allows the system to adjust to the specific electrical permittivity encountered for the oil and gas type used throughout testing. This procedure consists of filling the test section with oil only, to obtain the high permittivity point, and subsequently gas only, to obtain the low permittivity point. During each calibration, the measurements gathered are averaged over a short time span ($\approx 5s$) to ensure the calibrated capacitance values are not significantly disturbed by flow inconsistencies or measurement noise.

Procedure

For each test point conducted, the protocol was as follows. Firstly, the designated flowrates were achieved and allowed to settle within the optimum tolerance of the reference flowmeters. Once achieved, raw capacitance measurements were obtained for around 90 s for each test using the ECT system. After this, the capacitance data was checked to ensure no issues with connections or calibration were apparent, then the data analysis stage was completed offline, including: image reconstruction, cross-correlation, and the final data procedures outlined in this work.

3. Measurement method

Measurements obtained from ECT are used to reconstruct images within the pipe by LBP. The advantage of using this method is in its simplicity and fast processing rate. Although more advanced reconstruction methods are available, such as iterative based methods [26], LBP is specifically suited to this application, due to the relatively simple fluid geometry encountered in horizontal slug flows. Also, additional parameters needed for the more advanced methods (such as number of iteration steps) can cause artificial artifacts to appear within the image if an appropriate value is not used, which adds complexity to the process, especially over large ranges of flows.

Cross-correlation method

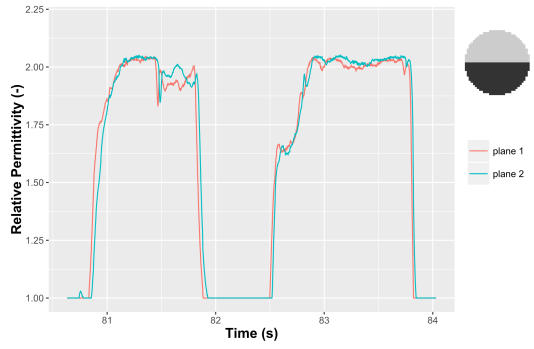

3.png

Figure 3: Example output from both measurement planes of the ECT system for two slugs passing through the sensor, forming the basis for cross-correlation. The signals represent the measured permittivity for the top half of the pipe cross-section only, indicated by the light grey area of the image in the top right.

Considering that fully reconstructed images of the flow are available through ECT, the cross-correlation process can be performed independently, in separate defined segments of the obtained cross-sectional images. The advantage of this is to allow the regions within the flow to be defined in terms of size and position, to specifically suit a particular structure of fluid passing the sensor [27]. This is of particular importance in ensuring that the measured velocity refers specifically to the speed of the passing slug, as opposed to wave propagation at the fluid/gas interface. Figure 3 displays a typical output from the ECT system. The relative permittivity is obtained from the normalised capacitance data and fluid properties, constrained to the area of the cross-sectional image, depicted in grey in the top left graphic. Two signals are present, one from each measurement plane, in which the time difference between the signals provides the basis for cross-correlation. The data has been reduced to show only two separate slugs passing through the sensor, which, due to the relatively high slug translational velocity, is necessary in order to clearly distinguish the two signals. For each cross-sectional zone created, the cross-correlation function can be described as:

$$R_{xy}(\tau) = \lim_{T\to\infty} \frac{1}{T} \int_0^T x(t)y(t+\tau)dt \tag{1}$$

where: $x(t)$ and $y(t)$ are the measured functions of permittivity (or relative density) in time, T is the length of time within the process and the region between 0, and T is the integration window for the selected data segment. At the maximum of this function ($R_{xy}(\tau)$), the corresponding value of τ is taken as the transit time of the body in question. The cross-correlation velocity, or in this work the measured slug translational velocity is given by:

$$U_{cc} = U_T = L/\tau \tag{2}$$

where U_T and L are the slug translational velocity and distance between sensor planes respectively. In this study, four separate correlation zone configurations are used, presented in Figure 4. The first (a), represents a full cross-

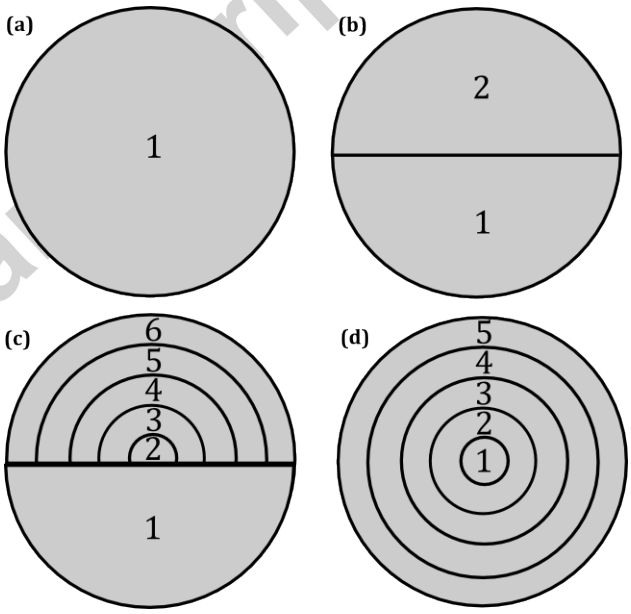

4.png

Figure 4: Configurations of cross-correlation zones (zone maps) used in this work.

section conventional setup, (b) is similar, with the main difference being that we can specifically select only the top half of the cross-section, giving a more sensitive signal to cross-correlate when the flow moves from stratified to slug. This ensures that the velocity of entrained gas in the film section of the flow is not included in the measurement. Zone (c), is an annular based map which only occupies the top half of the cross-section, giving similar advantages as those of (b), but allowing analysis of the flow profile. Lastly, (d) is a fully annular configuration which is used when the flow is axis-symmetric, with its specific use demonstrated in Section 4.

Different configurations of cross-correlation have been used in this study. Firstly, in line with conventional use,

a large integration window (5 s) is used to give a single averaged measurement for slug translational velocity over an entire data set. In this case, we consider multiple slug occurrences together, which represents a baseline similar to that used in other work. In order to measure specific slugs individually, the correlation window is decreased to a value similar to the slug duration, permitting an average velocity of individual slugs. Alternatively, the window can be decreased significantly (to $\sim 0.3s$ dependent on slug size). This allows two different measurements: the velocity of gas entrainment within the slug, but also, the independent measurement of both slug front and tail velocity. The final method described is assisted by cross-correlating the differential of the signal, i.e. with $x(t)$ and $y(t)$ in Eq. (1) replaced with $\frac{dx}{dt}$ and $\frac{dy}{dt}$.

Mixture velocity prediction

The ability to accurately measure the translational velocity of slugs is only of significance if it can be directly related to the phase flowrates. As pointed out by Dukler and Faber [28], by far the most popular method in use is that of the linear relation between slug translational velocity and the mixture superficial velocity suggested by [29], described as:

$$U_T = C_o J + U_{dj} \tag{3}$$

where: $J = J_g + J_l$ is the mixture superficial velocity, with J_g and J_L as the superficial gas and oil velocity respectively, C_o is the distribution parameter and U_{dj} is the drift velocity.

This relationship has received much attention by its application for the drift flux model [30, 31], and to the measurement of the speed of kinematic wave propagation through cross-correlation flowmeters [32]. Most work on this relationship concentrates on deriving expressions for both the distribution parameter C_o and the drift velocity U_{dj}. A crucial finding specifically for slug flows, was that of a critical mixture Froude number presented by Bendikson [33],

$$Fr_m = \frac{J_g + J_l}{\sqrt{\frac{\rho_l - \rho_g}{\rho_l} gD}} \tag{4}$$

where: D is the diameter and ρ_g and ρ_l are the gas and liquid densities respectively.

A critical value of 3.5 was given for which a change in velocity exists due to flow pattern transition. The following expressions will be used for prediction in this work, based on both the drift flux model [31], and the work of Bendikson [33], respectively.

$$C_o = 1.2 - 0.2\sqrt{\frac{\rho_g}{\rho_l}} \tag{5}$$

$$U_{dj} = 0.54\sqrt{gD} \tag{6}$$

$$\left\{ \begin{array}{ll} Fr_m \geq 3.5 \Rightarrow & Co = 1.2 - 0.2\sqrt{\frac{\rho_g}{\rho_l}} \\ Fr_m < 3.5 \Rightarrow & Co = 1.05 \end{array} \right\} \tag{7}$$

$$\left\{ \begin{array}{ll} Fr_m \geq 3.5 \Rightarrow & U_{dj} = 0 \\ Fr_m < 3.5 \Rightarrow & U_{dj} = 0.54\sqrt{gD} \end{array} \right\} \tag{8}$$

4. Results and discussion

Slug front structures

By analysing the ECT images at the fronts of the oil slugs encountered in the flows tested, it is possible to class them according to their appearance. By doing this, we can analyse the cross-correlation data for the different slug fronts, and by comparing to theoretical prediction of the translational velocity; infer the effects of the slug front appearance on the accuracy of measurement. Figure 5 depicts the 3 distinct slug front structures (a,b and c) encountered, and an example of a slug tail structure (d) which is reasonably consistent for all slugs.

To obtain the images, the segment of data covering the evolution from stratified flow to the main slug body (cross-section of oil with some entrainment) is isolated for the selected slugs. The 2D images for each timestep within this segment are stacked on a 3D axis, and finally the number of images are reduced to display the most significant transitions. The spacing between each image is adjusted to ensure a clear image of the structures. It is therefore important to note that the aspect ratio of the images are exaggerated, and do not represent a comparable length of the different structures, hence no units along the axis are given.

The colour maps for the images are chosen to provide clear distinctions between each stacked image as well as intermediate values. Areas of high permittivity fluid (oil) are shown in blue, whereas low permittivity fluid (gas) areas are transparent, which is required when images are presented in this way in order to observe the change in structure over time. As is typical in ECT images, the interface between the two fluids is represented by the green area, and defines a point in the cross-section where neither only oil or only gas is present. This exists for two main reasons: firstly, the electrodes measure over a small volume as opposed to just a 2D plane as the images suggest, therefore the sensor can measure axially separated oil and gas at the same point in the cross-section. Secondly, 'blurring' of the interface is a common trait of LBP image reconstruction, due to the assumptions made in the algorithm.

Figure 5 (a) illustrates a typically expected configuration, where the fluid rises vertically up through the cross-section, or from a more central position to form the liquid slug. The images also show that the predominantly oil areas (blue) remain stable at the bottom of the cross-section and build gradually to fill the intermediate areas. This structure is the most commonly observed within the data sets and corresponds to a stable slug motion. Fig-

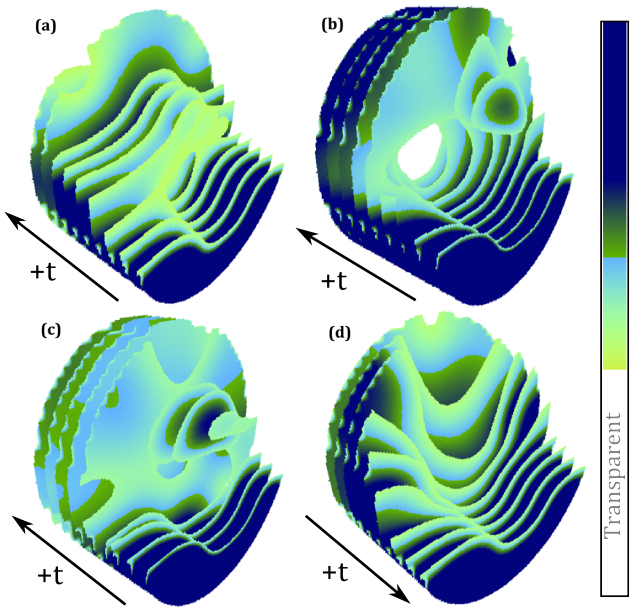

5.png

Figure 5: Stacked tomographic images illustrating the different types of slug front structures ((a),(b) and (c)) and slug tail structure (d)) encountered in the experiments covering the full flow range. Blue area indicates oil, green intermediate and transparent for gas.

ure 5 (b) depicts a gas core structure where an annulus of oil first appears, and the core subsequently fills shortly afterwards, with our preliminary measurements showing the annulus moving noticeably faster than the slug. As previously, the structure is relatively stable with only the initial core structures close to interfacial values (green areas), quickly replaced by high permittivity values. Figure 5 (c) displays an example of a more unstable structure, where an initial fluid structure, traveling faster than the slug, can appear from random locations within the cross-section. This can vary in its form, but can be categorised by its non-conformance. It is shown in this image that when the pipe cross-section is initially filled, much gas entrainment is present, portrayed by the green intermediate colour representation. This continues for much longer than the previous two structures, further indicating the instability, and providing justification for separating these slugs from the more stable types. Finally Figure 5 (d) shows the form of a typical liquid slug tail as the flow becomes stratified, this structure is relatively consistent for all tails observed in the tests. Due to its settling structure (inverse similarities to Figure 5 (a)), there is some difficulty in prescribing a suitable correlation zone map to represent the structures movement.

The objective of the following sections is to show that the slug structures identified previously can be used to identify which slugs represent, more accurately, the true translational velocity of the flow, and hence can be used to disqualify those deemed unrepresentative. Also, the structure should dictate the type of zone maps used for cross-correlation, to ensure that the slug body's movement itself is what is measured, as opposed to some entrainment or fluctuation at the liquid-gas interface. By using the combination of these two methods, a greater linearity between translational slug velocity and mixture velocity can be achieved, and therefore improved metering.

Velocity profiles

An initial method to provide some validation for using appropriate correlation zone maps for a particular slug front structure, can be achieved through obtaining velocity profiles. The most susceptible structure to this is the vertically rising structure depicted in Figure 5 (a). Due to its evolving structure, the zone map in Figure 4 (c) is used, with the number of zones increased to produce more in-depth profiles, and focusing on the top half of the pipe where change occurs. For a single test at $J_g = 2.19m/s$ and $J_l = 1.37m/s$, ECT data from five separate slug fronts, which fall into the category selected, are cross-correlated using the zone map stated. This provides an average velocity measurement for each vertical segment, which are plotted to provide the velocity profiles shown in Figure 6. The results are viable due to the known occurrence of wave structures in liquid slugs for industrial flows, where velocity increases when approaching the top or outer regions of the pipe, and levels out near the pipe wall. It is noted that the zone map area at the wall of the pipe will not portray the effects of wall shear stress due to the nature of the cross-correlation method. In comparison to other zone maps, which is found to be the most reliable. In some cases, where the structure rises as a flat surface rather than more centrally, it is found that a stratified based map gives a similar result, although as this is less common and the results so similar, the annular based zone map is deemed a better choice.

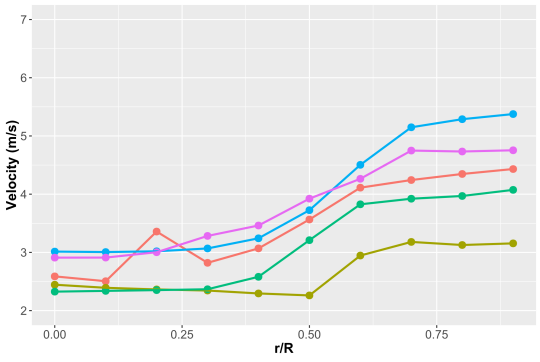

6.png

Figure 6: Measured axial velocity profile (top half of pipe only) of slug fronts. With different colours representing separate slugs in a single test, with slug fronts of type shown in Figure 5 (a), encountered during experiment at $J_g = 2.19m/s$ and $J_l = 1.37m/s$

Figure 7 displays the same method, but applied to the slug tail (as seen in Figure 5 (d)). As mentioned previously, the selected zone map does not necessarily match the structures dynamic behaviour, and therefore the viability of the profile is undermined. However, area-averaged results are comparable to the use of the zone map shown

in Figure 4 (b). Therefore, the same approach as previously is adopted to provide averaged velocity measurements of each zone map segment axially spaced along the top half of the pipe for multiple slugs from the same test ($J_g = 2.96m/s$ and $J_l = 1.025m/s$). The results, though not as stable as the previous test, seem to show an opposite behaviour, with the fluid in the top or at the walls of the top half of the pipe traveling relatively slowly, then accelerating as the centre point is approached. Finally,

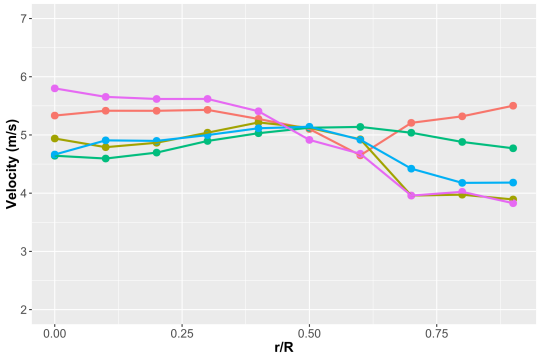

7.png

Figure 7: Measured axial velocity profile (top half of pipe only) of slug tails. With different colours representing separate slugs in a single test, with slug tails of type shown in Figure 5 (d), encountered during experiment at $J_g = 2.96m/s$ and $J_l = 1.025m/s$

Figure 8 illustrates a measured velocity profile of slugs with a gas core front structure, as seen in Figure 5 (b), measured by use of the zone map depicted in Figure 4 (d). In this case, cross-correlation velocity is measured in each annular segment, giving an axisymmetric velocity profile for multiple 'gas core' type slugs observed at $J_g = 0.98m/s$ and $J_l = 1m/s$. Such measurements become difficult due to the entrainment present, especially within the core, and ensuring only the main fluid body is measured is difficult to guarantee. Despite this, the result clearly shows a significant change between core and annulus which will be analysed in a later section. Also, a reduction of velocity near the top of the pipe is observed, this may be due to gas pockets around the pipe circumference, observable from the image.

For all the velocity profiles measured, good consistency between measured profiles of similar structures during the same test is achieved. All velocity profile plots have been displayed with the same velocity range to provide some comparison between the range of values encountered. A false origin of $2m/s$ is used to achieve this while maintaining a clear presentation of the data.

Selective measurement

In order to understand the effects of each slug structure type on the overall measurement, it is necessary to analyse each individual slug velocity (both front and tail) for a particular data set, and compare this to the prediction of translational velocity. It is noted that the theoretical prediction, although based on the reference measurements, is only expected to serve as a guideline of the true

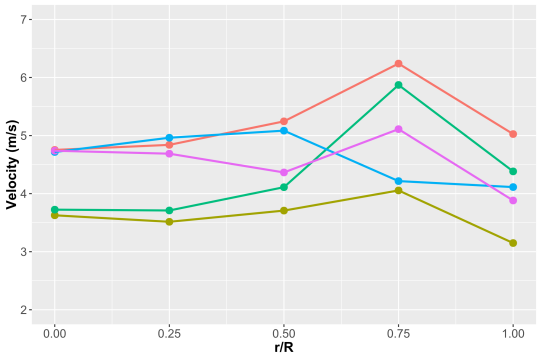

8.png

Figure 8: Measured axisymmetric velocity profile of slug fronts . With different colours representing separate slugs in a single test, with slug fronts of type shown in Figure 5 (b), encountered during experiment at $J_g = 0.98m/s$ and $J_l = 1m/s$

value, due to the inaccuracy present in the correlations. Also, due to the industrial scale flow experienced within the testing, reasonable deviation of the slug translational velocities with respect to their mean values is expected. Figure 9 (top) shows an example testpoint where the front and tail velocity (red and blue points respectively) of every slug encountered are plotted against time (as observed in the test), using the zone map depicted in Figure 4 (b). The mean of both front and tail velocities separately are also displayed by their corresponding coloured line, along with the theoretical prediction of slug translational velocity, displayed by the black line. It is assumed that the more representative the measurements are, the theoretical prediction (black line), will be closer to the centre between the mean front and tail velocities (red and blue lines).

Figure 9 (bottom) shows the same data as previously, except only slugs which exhibit stable rising structures (Figure 5 (a)) are included (selective measurement), with mean values adjusted to only include the measurements present. The results clearly show an improvement when selective measurement is conducted, where the prediction line sits closer to the centre of the front and tail mean velocities. This is mainly achieved, through the reduction in mean slug front velocity, which confirms the previously made statement that the interfacial instabilities move faster than the true translational velocity. Another observation which can be made is the benefit of averaging the front and tail velocities, as opposed to using either individually. This is important in reference to the tail velocities, as they are consistent in their structure, and thus obtaining a reliable measurement is easily achieved.

Behaviour of slug fronts and tails

A further way of analysing slug structural effects, is through the comparison of slug front and tail velocities. As pointed out by Abdulkadir *et al.* [34], relatively close values of slug front and tail velocity can be used as an indication of good flow development. Therefore, by categorising the different slug structures within a developed

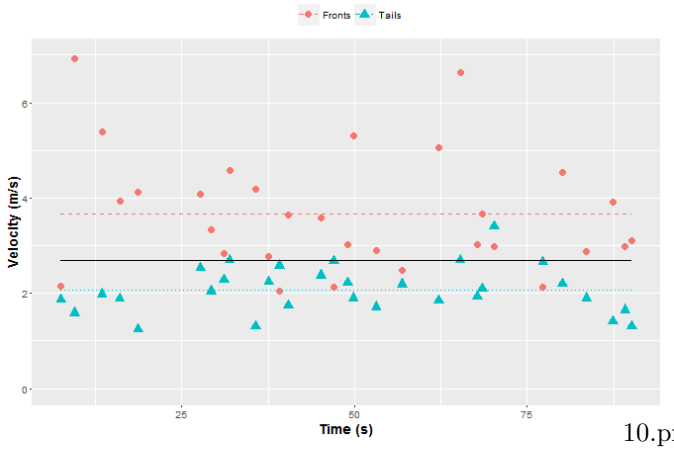

9 a.png

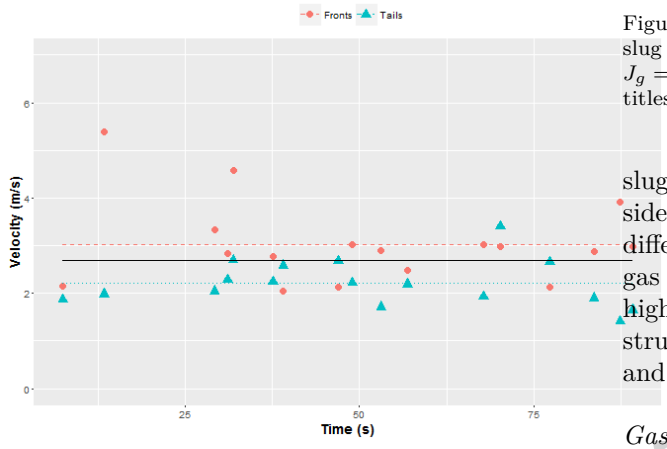

9 b.png

Figure 9: Slug front and tail velocities of multiple different slugs encountered at $J_g = 0.98m/s$ and $J_l = 1m/s$, for both: inclusive of all slugs (top) and inclusive of only slug fronts of type Figure 5 (a). Horizontal lines indicate: predicted translational velocity (U_T) (black), mean slug front velocity (red) and mean slug tail velocity (blue).

flow, the variation present for the different structures can be used as an indication of their stability, or degree of representation. Figure 10 shows a comparison between front and tail velocities of slugs chosen from four separate test-points (with flow range indicated in caption), covering the 3 slug front structures defined in Figure 5. The plot also gives an impression of the frequency of each structure type observed during testing . The results were gathered using the correlation zone map depicted in Figure 4 (b), with a small correlation window and by correlating the differential of the time series. This allowed individual slug velocity measurement, differentiation between front and tail velocities, as well as representing conventional cross-correlation. The black line in Figure 10 indicates where the front and tail velocities of a certain slug are equal, therefore, points above this line represent instances where the front is higher than the tail velocity (i.e. acceleration). The results show that the most frequent structure type (stable rise (a)) produces the most consistent similarity between slug front and tail velocity. Though they indicate that the majority of

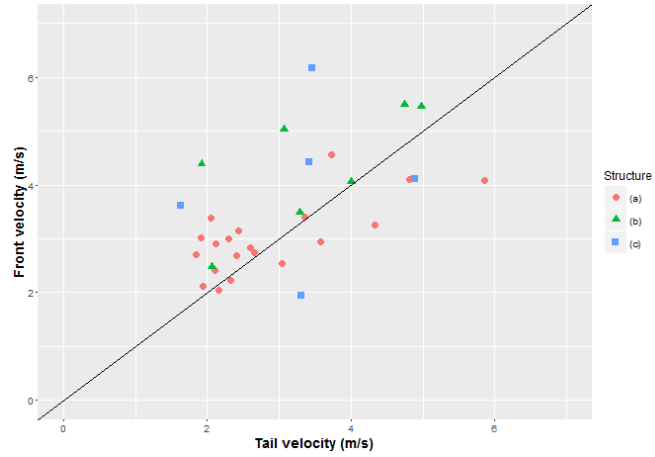

10.png

Figure 10: Comparison of slug front and tail velocities for different slug front structures in 3 separate test points covering flow range of $J_g = 0.47m/s$ to $2.19m/s$ and $J_l = 1.37m/s$ to $1.522m/s$. Structure titles refer to those seen in Figure 5.

slugs within this category are accelerating, this is not considered a problem with respect to flow development, as the differences in values are relatively small. Structures with gas cores (b) have a larger variation, with a clear bias for higher front velocities, as expected. Finally, the unstable structures also produce a higher variation between front and tail velocities, with no clear bias.

Gas core structures

As mentioned previously, slug fronts with a gas core, when measured using the correlation zone maps used for other structures, tend to overestimate the translational velocity significantly. This can be explained because the cross-correlation includes the oil annulus as the majority of the measurement, where this structure is propelled around the pipe circumference at a greater velocity. In order to counter this, it is assumed that the only part of the structure which is truly representative of the slug, is the central core zone, when it eventually fills the cross-section. Therefore the most suitable zone map to apply to these slug types would be a conventional annular type, as shown in Figure 4 (d), whilst only considering the zones which encompass the core area. The results in Figure 11 are measurements of gas core structure slugs using both the annular zone map, only considering zone segments that encompass the core area (annular - centre zones) as well as cross-correlating the entire cross-section (Figure 4 (a)) named as conventional.

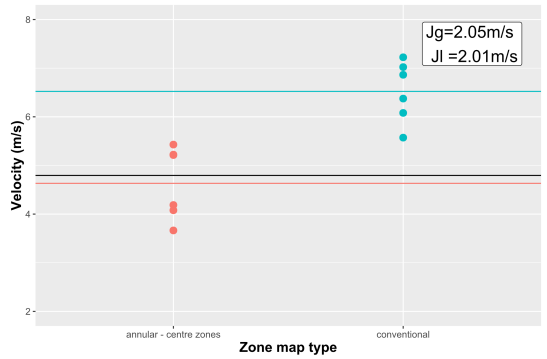

11 a.png

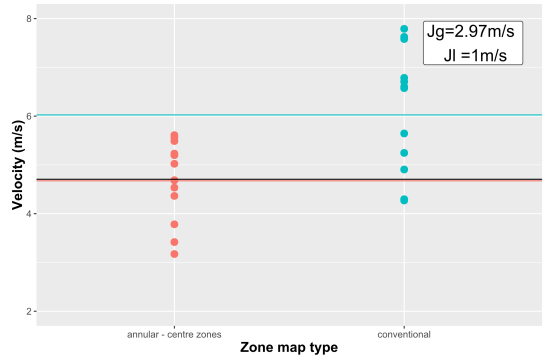

11 b.png

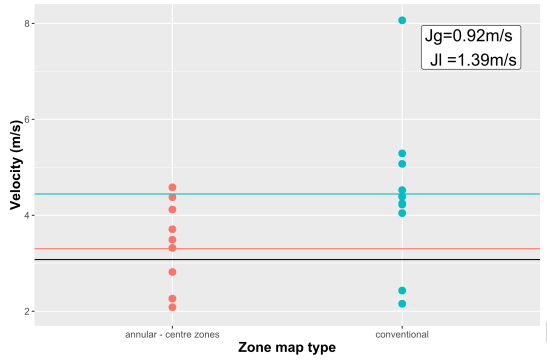

11 c.png

Figure 11: Comparison of individual gas core structure slug front velocities observed during the three separate experiments indicated in each plot. Measured through conventional averaged cross-correlation and using an annular based zone map whilst only taking measurements from the central core zones. Horizontal lines represent: predicted translational velocity (U_T) (black), averaged values (red and blue).

The results show that the average velocity value obtained when only using the central zones decreases, and obtains a figure much closer to the expected. This is due to the reasons explained previously and provides a viable solution to measuring the slug translational velocity for these slug types. However, an important point is that, due to the smaller region of measurement, it is reasonable to assume that the reliability of the measurement is somewhat reduced, due to the possibility of some discontinuity or instability within the core region having more effect during such measurements. Despite this, the presented method displays better measurement potential in comparison to the conventional technique of cross-correlation of the entire measured cross-section, with reference to Figure 4 (a).

Accuracy comparison

To determine if an improvement in accuracy is possible through the selective based measurement method presented here, the mixture velocity can be determined from the measurements for the following different methods:

1. Conventional cross-correlation is tested by applying the zone map presented in Figure 4 (a), with a large integration window, giving a single velocity measurement for the data set.
2. The window is reduced to allow individual slug velocity measurement (inclusive of both front and tail) with averaged values.
3. A small window is combined with cross-correlation of the differential, zone map depicted in Figure 4 (b), measuring only front structures within category Figure 5 (a), and the front velocities are solely used.
4. An average of front and tail velocities of the previous method.

Figure 12 displays the results for this test, along with predictions outlined in Eq (3) through Eq (8). It is noted that the more complex zone map used previously for obtaining velocity profiles (Figure 4 (c)), is not included here. This is due to results for the selective based methods (3 and 4), (referring to methods which exclude slugs based on their front structures), giving similar averaged results when using either zone map depicted in Figure 4 (b) or (c).

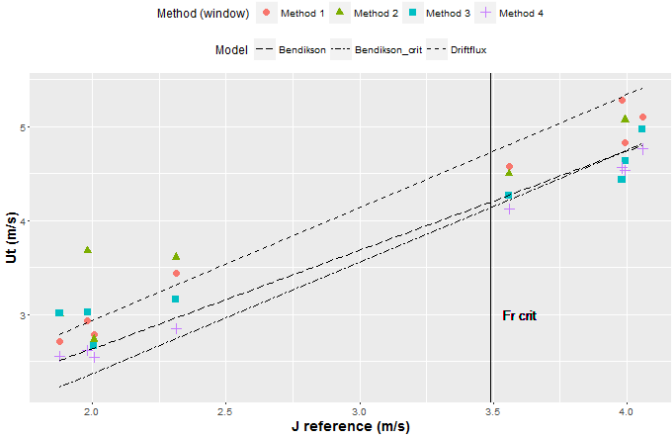

12.png

Figure 12: Comparison of accuracy encountered for the different methods of cross-correlation and zone maps covering all experiments. Along with previously derived predictions.

Both axis ranges have been restricted to only cover the values observed in the tests, this is to ensure that the results from the different methods can be compared easily, considering that the differences are relatively small. The results, overall, show correlation between measurements and theoretical predictions for all methods, with method 4 producing the most reliable linear trend. Firstly, the conventional method (1) gives a relatively good linear trend, though variation is reasonably large, and comparable to results from other non-intrusive devices [22, 8]. Method (2)

gives a similar trend but with some data points with larger variation, this can be explained due to unstable slugs having a more profound effect on the measurement when considered individually. Both method (1) and (2) give slightly higher results than the others, due to the inclusion of less stable structures with larger velocities at the slug front. They may also be affected by not distinguishing between front and tail. Method (3) shows overall lower values but with similar variation to method (1). Finally, the selective method with average front and tail velocities (4) gives the best result. The linear trend is strong with reduced variation, the data points suggest good correlation with the prediction of Bendikson [33], including the critical Froude number boundary.

Method (4) can now be presented in terms of measurement and reference as illustrated in Figure 13. In this plot, the reference mixture superficial velocity is obtained from the reference flowmeters as in Figure 12 ($J_{ref} = \frac{Q_{g-ref}+Q_{l-ref}}{A}$), and the measured mixture superficial velocity is obtained by rearranging Eq (3), and using values of the distribution parameter C_o and drift velocity U_{dj} from Eq (5) through Eq (8), with reference to Eq (4).

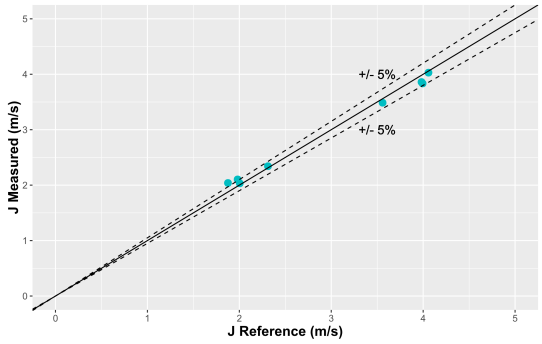

13.png

Figure 13: Results of applying method (4) and prediction of Bendikson [33] to the measurement of the mixture velocity for all test points. Compared to reference measurements of the mixture velocity recorded during testing.

The result shows a good linear trend, where the majority of data points are well within a +/-5% error range, and close resemblance to the prediction. Measured points at the lower values of mixture superficial velocity (<2m/s) appear to have slightly higher error margins, as seen by Zhang and Dong [22], though more data would be required to confirm this. Such results are comparable to advanced metering methods such as ultrasonic doppler sensors [9] which measure the actual velocity of fluid particles. The method represented, therefore, provides a basis for ECT cross-correlation flowmeters to compete with other methods which are less suitable to oilfield applications.

5. Conclusion

ECT measurements were taken for a range of two-phase oil and gas slug flows in a horizontal pipe. Constructed images were used to analyse the slug front structures and determine their individual suitability for measurement of slug translational velocity. The results provide the following conclusions:

- Slug front structures can be categorised broadly into three groups, two of which are susceptible to accurate cross-correlation.
- Slug tail structures are more consistent in their shape, with only a single stable type identified throughout the tests conducted.
- By selecting appropriate zone maps for a given structure, velocity profiles can be obtained along certain symmetrical axis depending on the type of slug structure present.
- Gas core and unstable slug front structures travel at a higher velocity than the slug translational velocity and therefore can be detrimental to cross-correlation type metering.
- The removal of slugs with unstable front structures can give results more representative of the slug translational velocity.
- When measured conventionally, unstable and gas core structures show more disparity between front and tail velocities.
- Slugs with gas core front structures are more representative if only the central zones (using an annular based map) are measured, though this may compromise their reliability.
- By using selective measurement, differential based cross-correlation and the average velocity of slug front and tail, measurements of mixture superficial velocity can be obtained within +/-5%.

To improve upon this work, more data can be gathered at a greater resolution over the flow range, including testing for vertical pipes. This would provide greater clarification of the obtainable accuracy, but would also demonstrate the effect of flow parameters and fluid properties on the frequency of the different slug front structures observed in this work. Furthermore, in order to recover gas and oil superficial velocities (especially for unstable flows where the unit cell approach becomes difficult [35]), full automation of this process is required, where for each slug, structure identification is carried out, and the corresponding cross-correlation algorithm is applied.

6. References

[1] Abraham E. Dukler and Martin G. Hubbard. A Model for Gas-Liquid Slug Flow in Horizontal and Near Horizontal Tubes. *Industrial and Engineering Chemistry Fundamentals*, 14(4):337–347, 1975.

[2] Simon Pedersen, Petar Durdevic, and Zhenyu Yang. Challenges in slug modeling and control for offshore oil and gas productions: A review study. *International Journal of Multiphase Flow*, 88:270–284, 2017.

[3] Abdalellah O. Mohmmed, Mohammad S. Nasif, Hussain H. Al-Kayiem, and Rune W. Time. Measurements of translational slug velocity and slug length using an image processing technique. *Flow Measurement and Instrumentation*, 50:112–120, 2016.

[4] M.A. Alssayh, A. Addali, and D. Mba. Determining slug velocity in two-phase flow with acoustic emission. *51st Annual Conference of the British Institute of Non-Destructive Testing 2012, NDT 2012*, 0044(0), 2012.

[5] R. Van Hout, D. Barnea, and L. Shemer. Translational velocities of elongated bubbles in continuous slug flow. *International Journal of Multiphase Flow*, 28(8):1333–1350, 2002.

[6] Netaji R. Kesana, Mazdak Parsi, Ronald E. Vieira, Barry Azzopardi, Eckhard Schleicher, Brenton S. McLaury, Siamack A. Shirazi, and Uwe Hampel. Visualization of gas-liquid multiphase pseudo-slug flow using Wire-Mesh Sensor. *Journal of Natural Gas Science and Engineering*, 46:477–490, 2017.

[7] Wael H. Ahmed. Capacitance sensors for void-fraction measurements and flow-pattern identification in air-oil two-phase flow. *IEEE Sensors Journal*, 6(5):1153–1163, 2006.

[8] L. S. Zhai, N. D. Jin, Z. K. Gao, A. Zhao, and L. Zhu. Cross-correlation velocity measurement of horizontal oil-water two-phase flow by using parallel-wire capacitance probe. *Experimental Thermal and Fluid Science*, 53:277–289, 2014.

[9] Xiaoxiao Dong, Chao Tan, Ye Yuan, and Feng Dong. Measuring Oil-Water Two-Phase Flow Velocity with Continuous-Wave Ultrasound Doppler Sensor and Drift-Flux Model. *IEEE Transactions on Instrumentation and Measurement*, 65(5):1098–1107, 2016.

[10] C.T. Crowe. *Multiphase Flow Handbook*. Mechanical and Aerospace Engineering Series. CRC Press, 2005.

[11] I. Ismail, J.C. Gamio, S.F.A. Bukhari, and W.Q. Yang. Tomography for multi-phase flow measurement in the oil industry. *Flow Measurement and Instrumentation*, 16(2-3):145–155, 2005.

[12] Antoine Dupre, Guillaume Ricciardi, Salah Bourennane, and Saba Mylvaganam. Electrical Capacitance Based Flow Regimes Identification - Multiphase Experiments and Sensor Modelling. *IEEE Sensors Journal*, (c):1–1, 2017.

[13] Laurent F.C Jeanmeure, Tomasz Dyakowski, William B.J Zimmerman, and Wayne Clark. Direct flow-pattern identification using electrical capacitance tomography. *Experimental Thermal and Fluid Science*, 26(6-7):763–773, 2002.

[14] W. Q. Yang and M. S. Beck. An intelligent cross correlator for pipeline flow velocity measurement. *Flow Measurement and Instrumentation*, 8(2):77–84, 1998.

[15] M.S. Beck and A. Pląskowski. *Cross Correlation Flowmeters, Their Design and Application*. Taylor & Francis, 1987.

[16] F. Dong, Y. B. Xu, L. J. Xu, L. Hua, and X. T. Qiao. Application of dual-plane ERT system and cross-correlation technique to measure gas-liquid flows in vertical upward pipe. *Flow Measurement and Instrumentation*, 16(2-3):191–197, 2005.

[17] J. M. Elmy, L. M A Hanis, A. R. Ruzairi, and M. F M Omar. Real-time velocity profile measurement in two-phase oil/gas flow by twin-plane segmented ECT system. *Conference Record - IEEE Instrumentation and Measurement Technology Conference*, 2015-July:1567–1572, 2015.

[18] Y. Mi, M. Ishii, and L. H. Tsoukalas. Investigation of vertical slug flow with advanced two-phase flow instrumentation. *Nuclear Engineering and Design*, 204(1-3):69–85, 2001.

[19] Lev Shemer. Hydrodynamic and statistical parameters of slug flow. *International Journal of Heat and Fluid Flow*, 24(3):334–344, 2003.

[20] Priscilla M. Ujang, Christopher J. Lawrence, Colin P. Hale, and Geoffrey F. Hewitt. Slug initiation and evolution in two-phase horizontal flow. *International Journal of Multiphase Flow*, 32(5):527–552, 2006.

[21] Eissa Al-Safran, Gene Kouba, and James P. Brill. Statistical analysis and hydrodynamic modeling of unsteady gas-liquid slug velocity behavior. *Journal of Petroleum Science and Engineering*, 109:155–163, 2013.

[22] F Zhang and F Dong. A measurement method of slug flow velocity of gas-liquid two-phase flow in horizontal pipe. *2010 IEEE Instrumentation Measurement Technology Conference Proceedings*, pages 250–254, 2010.

[23] Emerson dos Reis and Leonardo Goldstein. A non-intrusive probe for bubble profile and velocity measurement in horizontal slug flows. *Flow Measurement and Instrumentation*, 16(4):229–239, 2005.

[24] Wael H. Ahmed. Experimental investigation of air-oil slug flow using capacitance probes, hot-film anemometer, and image processing. *International Journal of Multiphase Flow*, 37(8):876–887, 2011.

[25] Andrew Hunt. Weighing without touching: Applying electrical capacitance tomography to mass flowrate measurement in multiphase flows. *Measurement and Control (United Kingdom)*, 47(1):19–25, 2014.

[26] Øyvind Isaksen. A Review of Reconstruction Techniques for Capacitance Tomography. *Measurement Science and Technology*, 7(3):325–337, 1999.

[27] B. J. Azzopardi, L. A. Abdulkareem, D. Zhao, S. Thiele, M. J. da Silva, M. Beyer, and A. Hunt. Comparison between electrical capacitance tomography and wire mesh sensor output for air/silicone oil flow in a vertical pipe. *Industrial & Engineering Chemistry Research*, 49(18):8805–8811, sep 2010.

[28] Abraham E. Dukler and J. Fabre. Gas Liquid Slug Flow - Knots and Loose Ends. *3rd International Workshop Two-Phase Flow Fundamentals*, (January 1994):355–469, 1994.

[29] M. K. Nicholson, K. Aziz, and G. A. Gregory. Intermittent two phase flow in horizontal pipes: Predictive models. *The Canadian Journal of Chemical Engineering*, 56(6):653–663, 1978.

[30] N. Zuber and J. A. Findlay. Average volumetric concentration in two-phase flow systems. *Journal of Heat Transfer*, 87(4):453–468, 1965.

[31] M. Ishii and T. Hibiki. *Thermo-fluid Dynamics of Two-Phase Flow*. 2nd ed. edition, 2006.

[32] G.P. Lucas and I.C. Walton. Flow rate measurement by kinematic wave detection in vertically upward, bubbly two-phase flows. *Flow Measurement and Instrumentation*, 8(3):133 – 143, 1998.

[33] Kjell H. Bendiksen. An experimental investigation of the motion of long bubbles in inclined tubes. *International Journal of Multiphase Flow*, 10(4):467 – 483, 1984.

[34] M. Abdulkadir, V. Hernandez-Perez, I.S. Lowndes, B.J. Azzopardi, and E. Sam-Mbomah. Experimental study of the hydrodynamic behaviour of slug flow in a horizontal pipe. *Chemical Engineering Science*, 156:147–161, 2016.

[35] G.B. Wallis. *One-dimensional two-phase flow*. McGraw-Hill, 1969.